Proceedings of the 8th WSEAS Int. Conference on Automatic Control, Modeling and Simulation, Prague, Czech Republic, March 12-14, 2006 (pp54-62)

Image Based System Identification

DEACHA PUANGDOWNREONG[*], and SARAWUT SUJITJORN[**]
[*] Department of Electrical Engineering, Faculty of Engineering
South-East Asia University
19/1 Petchkasem Road, Nongkham District, Bangkok, 10160
THAILAND
http://www.sau.ac.th
[**] School of Electrical Engineering, Institute of Engineering
Suranaree University of Technology
111 University Avenue, Muang District, Nakhon Ratchasima, 30000
THAILAND
http://www.sut.ac.th

Abstract: - Conventional identification needs system input and output recorded by sensors. In some situations, installation of a conventional sensor may be difficult or not possible due to hazardous environment and/or confined area. This paper proposes a new approach to system identification via image processing techniques. This approach permits non-intrusive and remote identification. One or more cameras can be an alternative to conventional sensors. Dynamical information of the system can be extracted from the recorded images. Details of information extraction from images are presented in this paper. For linear models, conventional identification techniques based on regression analysis are applied. For nonlinear models, the adaptive tabu search (ATS), one of the AI search techniques, is employed. The proposed approaches have been tested against the cart-plus-pendulum (CPP) system, and the vibrating tube system (VTS), respectively. Practical results have been achieved with high satisfaction.

Key-Words: - system identification, image processing, adaptive tabu search, cart-plus-pendulum system, vibrating tube system

1 Introduction

Model identification generally requires the knowledge of input and output of the system of interest. Input is often known and recorded because it is generated by a source. Recording output is not always possible in some situations because of harzard, unreachable location, too small of the area for sensor's installation, for example. This is because most of traditional sensors are intrusive, at least to the extent that they must be physically attached to the object's surface and require extensive wiring for data acquisition. Providing the system's dynamic behavior can be observed by human eyes, model identification will be possible by using a camera to record a sequence of the system's images. The data representing the system dynamic can be extracted from the recorded images using available image processing techniques. Then, the model identification can be accomplished based on the extracted data and the recorded input.

Research on dynamic motion of objects extracted from the sequence of images emerged in the 70s. During the 80s, the identification of an object's position and orientation in space started to appear [1-3]. The work [4] utilized images from a satellite to predict the glacier flow. The attempts in [5,6] came close to model identification but they were intended for machine vision that required the knowledge of object's orientation. In 2003, we proposed our approaches to identify dynamic model parameters by using the images recorded by a digital VDO camera [7]. Later, similar approaches to identify nonlinear mechanical systems were reported in 2004 [8].

This paper is proposed to fulfill our approaches to identify model parameters via image processing techniques. It is divided into five sections. Problem formulation appears in section 2. Section 3 provides the mathematical models of the tested systems, i.e. the cart-plus-pendulum (CPP) system, and the vibrating tube system (VTS). Identification through image processing for linear and nonlinear parametric models of the CPP system, and partial differential equation (PDE) models of the VTS is explained in section 4. Section 5 of the paper gives the conclusion, while the adaptive tabu search is briefly described in the Appendix.

2 Problem Formulation

Identification of model parameters conventionally utilizes the input and output information of the system. The input can be deterministic, such as step, sinusoid, etc., or random. A traditional sensor is normally used to monitor the system output. The input and output data are fed to identification algorithm that in turn provides model parameters. This practice is represented by the diagram in Figure 1.

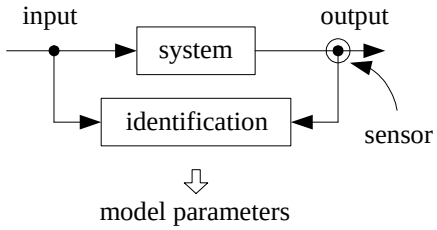

Fig. 1 Conventional identification approach.

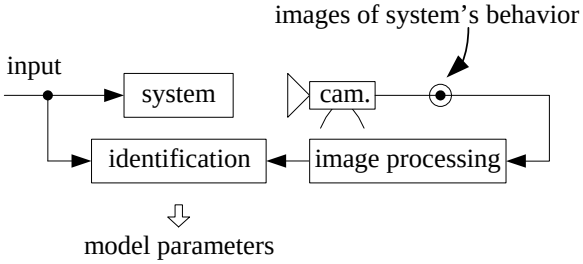

Fig. 2 Identification via image processing.

Under some circumstances where installation of traditional sensors is not possible as previously described, a camera can be used instead as shown in Figure 2. This is practical when the system's behavior can be easily observed by human eyes. The camera substitutes the function of the human eyes. With very rapid system dynamic so that it cannot be observed by human eyes, dynamic identification via image techniques is still possible with aids of a high performance acquisition system, and a complex image processing technique. This paper's discussion is confined to the first case, i.e. the system's behavior can be easily observed by human eyes. A digital VDO camera is employed to provide a sequence of images that capture the system dynamic. These images are passed through a suitable image processing algorithm. The image processing algorithm provides output ready for feeding the identification algorithm to compute the model parameters.

3 Mathematical Models

The systems under tests are the CPP system and the VTS. Their mathematical models are presented as follows.

3.1 Cart-plus-Pendulum (CPP) System

The CPP system is represented by the diagram in Figure 3. The system has a non-uniform force, *f*, exciting the cart. This force is generated by a motor and transmitted through a flexible belt. The belt motion consists of at least three modes, i.e. longitudinal (left-right), up-down swing, and sway depending upon the motor input, *u*. Refering to Figure 3, y = cart position, ϕ = angles of pendulum oscillation, M = cart mass (not known), f = force exerted by belt (not known), m = pendulum mass = 0.251 kg., l = length of pendulum rod = 0.4 m, and g = gravity = 9.81 m/s^2. The pendulum rod is assumed to be weightless.

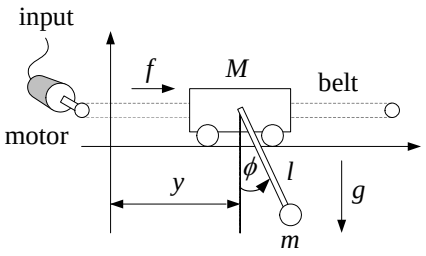

Fig. 3 The cart-plus-pendulum system.

Derivation of the models is based on Lagrange's equation of motion [9]. Lagrange's function, $L(\cdot)$, represents the difference between the kinetic energy, $K(\cdot)$, and the potential energy, $V(\cdot)$, as shown in (1).

$$L(\phi, y, \dot{\phi}, \dot{y}) = K(\phi, y, \dot{\phi}, \dot{y}) - V(\phi) \tag{1}$$

$$K(\cdot) = \frac{1}{2} M (v_{\text{cart}})^2 + \frac{1}{2} m (v_{\text{pend}})^2 \tag{2}$$

The kinetic energy composes of the energy of the cart and the pendulum as expressed by (2), in which $v_{\text{cart}} = \dot{y}$, and $v_{\text{pend}} = (\dot{y} + l\cos\phi\dot{\phi}, l\sin\phi\dot{\phi})$. Hence, the equation (2) can be rewritten as (3).

$$K(\cdot) = \frac{1}{2}[\dot{\phi}, \dot{y}] \begin{bmatrix} ml^2 & ml\cos\phi \\ ml\cos\phi & M+m \end{bmatrix} \begin{bmatrix} \dot{\phi} \\ \dot{y} \end{bmatrix} \tag{3}$$

For the potential energy when the pendulum is at down-right position as shown in Figure 3, $V(\phi) = -mgl\cos\phi$. Thus, Lagrange's function for the CPP system can be expressed by (4), where $\alpha = ml^2$, $\beta = ml$, $\gamma = (M+m)$, and $D = mgl$, respectively.

Consequently, we can obtain the angular momentum, p_ϕ, and the momentum in the

longitudinal direction, p_y, as (5) and (6), respectively.

$$L(\phi, y, \dot{\phi}, \dot{y}) = \frac{1}{2}\left[\alpha(\dot{\phi})^2 + 2\beta\cos\phi\dot{y}\dot{\phi} + \gamma(\dot{y})^2\right] + D\cos\phi \quad (4)$$

$$p_\phi = \frac{\partial L}{\partial \dot{\phi}} = \alpha\dot{\phi} + \beta\cos\phi\dot{y} \quad (5)$$

$$p_y = \frac{\partial L}{\partial \dot{y}} = \gamma\dot{y} + \beta\cos\phi\dot{\phi} \quad (6)$$

When there is only the force, f, applied to the cart, i.e. no external force applied directly to the pendulum, the motion of the CPP system can be described by Lagrange's equations of motion as shown in (7) and (8).

$$\frac{d}{dt}\frac{\partial L}{\partial \dot{\phi}} - \frac{\partial L}{\partial \phi} = 0 \quad (7)$$

$$\frac{d}{dt}\frac{\partial L}{\partial \dot{y}} = f \quad (8)$$

From (7) and (8), we can obtain (9) and (10), respectively.

$$\alpha\ddot{\phi} + \beta\cos\phi\ddot{y} + D\sin\phi = 0 \quad (9)$$

$$\gamma\ddot{y} + \beta\cos\phi\ddot{\phi} - \beta(\dot{\phi})^2\sin\phi = f \quad (10)$$

By substituting α, β, γ, and D into the equations (9) and (10), the equations of motion (11) and (12) are obtained.

$$\ddot{\phi} = \frac{f\cos(\phi) + 0.5ml\sin(2\phi)(\dot{\phi})^2 + (M+m)g\sin(\phi)}{l\left[m\cos^2(\phi) - (M+m)\right]} \quad (11)$$

$$\ddot{y} = \frac{f + 0.5mg\sin(2\phi) + ml\sin(\phi)(\dot{\phi})^2}{\left[(M+m) - m\cos^2(\phi)\right]} \quad (12)$$

Unknown system parameters, M and the expression of the non-uniform force, f, as a function of the motor input, u, need to be identified.

3.2 Vibrating Tube System (VTS)

The diagram of the VTS is represented by Figure 4. With motor's random input, the tube motion consists of at least three modes, i.e. clockwise-counterclockwise rotation, up-down swing, and sway. The dynamic behavior of this system in 3D-space can be represented by the PDE models. To obtain such the PDE models, the VTS could be considered in two separate planes, i.e. *x-y* plane, and *y-z* plane as shown in Figure 5, where $z(x,y,t)$ = tube position in the z axis, u = motor input, K_M = motor gain (not known), K_D = driver gain (not known), and gravity g_y = 9.81 m/s^2. The tube position, $z(x,y,t)$, is varied to the position in the x axis, the y axis, and time (t).

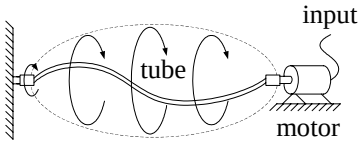

Fig. 4 The vibrating tube system.

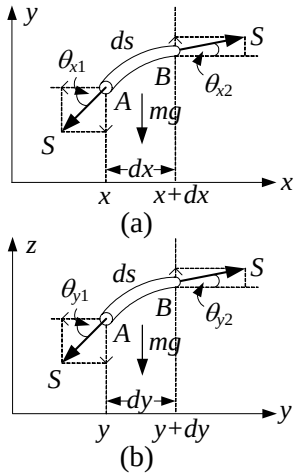

Fig. 5 Section of the tube considered in two planes, (a) *x-y* plane (b) *y-z* plane.

On the basis of vibrating string and membrane models [10], the mathematical models of the VTS can be developed. Regarding to the Newton's law of motion, the summation of force, S, acting on the tube along the x and y axes in Figure 5(a) can be obtained as expressed in (13) and (14), respectively.

$$\sum S_x = S\cos\theta_{x2} - S\cos\theta_{x1} \quad (13)$$

$$\sum S_y = S\sin\theta_{x2} - S\sin\theta_{x1} - mg \quad (14)$$

When θ_{x1} and θ_{x2} are very small, we can approximate $\cos\theta_{x1} \cong \cos\theta_{x2}$. Thus, equation (13) is equal zero. This means that there is no force acting on the tube along the x axis. In this case, $\sin\theta_{x1} \cong \tan\theta_{x1}$, and $\sin\theta_{x2} \cong \tan\theta_{x2}$. Thus, equation (14) can be written as (15).

$$\sum S_y = S\tan\theta_{x2} - S\tan\theta_{x1} - mg$$

$$\sum S_y = S\left[\left(\frac{\partial z}{\partial x}\right)_B - \left(\frac{\partial z}{\partial x}\right)_A\right] - mg \quad (15)$$

The slope at point *B* of the tube in Figure 5(a) is approximated by two terms of the Taylor series as shown in (16).

$$\left(\frac{\partial z}{\partial x}\right)_B \cong \left(\frac{\partial z}{\partial x}\right)_A + \left(\frac{\partial^2 z}{\partial x^2}\right)_A dxdy \tag{16}$$

By substituting (16) into (15), the summation of force, *S*, acting on the tube along the *y* axis is obtained as shown in (17).

$$\sum S_y = S\left(\frac{\partial^2 z}{\partial x^2}\right)dxdy - mg \tag{17}$$

$$\sum S_z = S\left(\frac{\partial^2 z}{\partial y^2}\right)dxdy - mg \tag{18}$$

In similar fashion, when the tube as shown in Figure 5(b) is considered in the *y*-*z* plane, the summation of force, *S*, acting on the tube along the *z* axis is obtained as shown in (18), since there is no force acting on the tube along the *y* axis.

σ is defined as the tube mass per unit length in both *x* and *y* axes. If $ds \cong dx \cong dy$, then $m = \sigma dxdy$. By applying the Newton's law, summation of force, *S*, can be provided by (19). The overall force acting on the tube is expressed in (20).

$$\sum S = \sigma dxdy \frac{\partial^2 z}{\partial t^2} \tag{19}$$

$$\sum S = \sum S_y + \sum S_z \tag{20}$$

By substituting (17), (18), and (19) into (20), the generalized models of the VTS based on the wave equation can be obtained as shown in (21), while the applied force, *S*, as the function of the motor input, *u*, is expressed in (22). Three system parameters, σ, K_M, and K_D, need to be identified.

$$\frac{\partial^2 z}{\partial t^2} = \frac{S}{\sigma}\left(\frac{\partial^2 z}{\partial x^2} + \frac{\partial^2 z}{\partial y^2}\right) - g_y \tag{21}$$

$$S = K_D K_M u \tag{22}$$

4 Identification via image processing

This section describes our approaches to system identification via image processing techniques for the CPP system and the VTS.

4.1 Identification of the CPP System

The effectiveness of our approach is firstly demonstrated on the CPP system represented by Figure 6. A VDO camera was installed in perpendicular to the belt. Thus, the plane captured by the camera contains the traverse motion of the cart, and the swinging motion of the pendulum. The camera is Panasonic DVC-PRO25 (AJ-D400) having its lens of 6.5-123 mm. The pendulum swang within 2 ranges: ±0.2 and ±0.6 rad. The camera captured the motion images simultaneously to the sensor reading angles of oscillation, ϕ. The sampling interval for the sensor was 0.15 sec. The image files (VDO tapes) were converted to ".avi" files, and then to ".bmp" files. The time interval between two consecutive images is equivalent to a sampling interval of 0.0735 sec. which is finer than that provided by the sensor. The system's sequence of images is captured, and further processed to extract the most necessary information for the system identification, i.e. cart positions, and pendulum angles of oscillation. For each frame of image, the position of each interested object must be separately and simultaneously located.

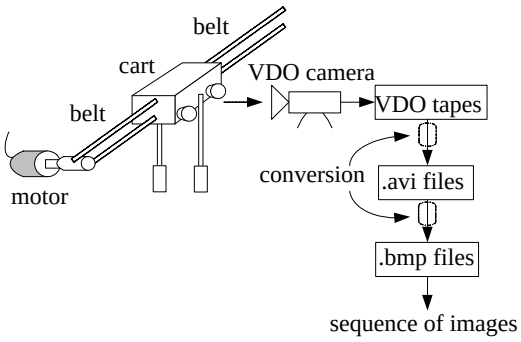

Fig. 6 The CPP system set-up.

To locate each object of the CPP system in image sequences, color segmentation technique is employed. There are five objects in the scene that need separate detections. These objects are background, reference point, pendulum, cart, and track. Different colors are assigned to each object. The simple color segmentation technique is then applied to segment out each object from the scene. By choosing different color ranges for each object, we are be able to separately locate all five objects and label each of them in every single image frame.

The image sequence is recorded in RGB format. Ranges of R, G and B values are firstly calculated for each object's color. The color threshold technique is applied to segment each object using these RGB parameters. Figure 7 shows the results of the color segmentation. From the segmented image, the position of the object (in pixel unit) is computed

with reference to its center of gravity. Finally, this position information is converted into the CPP system parameters which are cart positions, and pendulum angles of oscillation, ϕ.

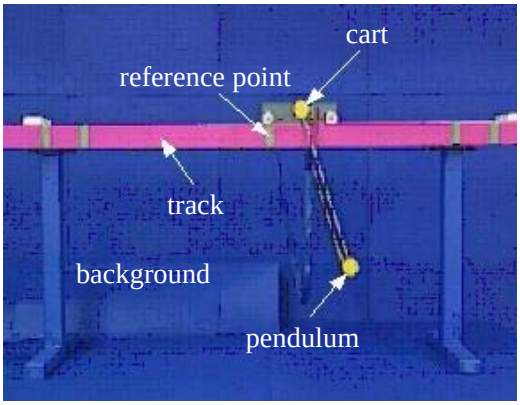

(a)

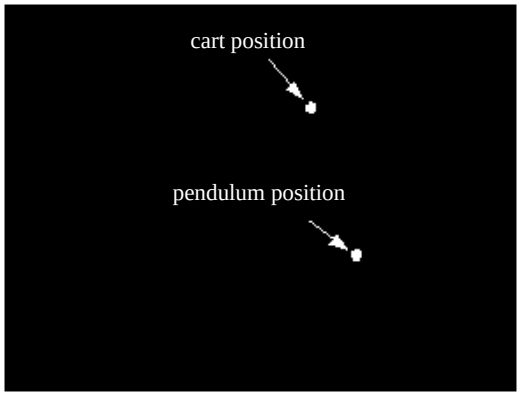

(b)

Fig. 7 Color segmentation of the CPP system, (a) recorded image (b) segmented image.

Due to imperfect lens, the recorded images are always distorted. To correct the distortion errors, the least square error (LSE) method is applied. After correction, the image data, pendulum angles of oscillation, agree with sensory data. To compare the sensory data with the uncorrected and the corrected image data, some results are plotted as shown in Figure 8.

To identify the CPP system parameters, the system was considered linear and nonlinear, respectively, according to the amplitude of the oscillation angles, ϕ. The results of the models obtained from the corrected image data are compared with those obtained from the sensory data.

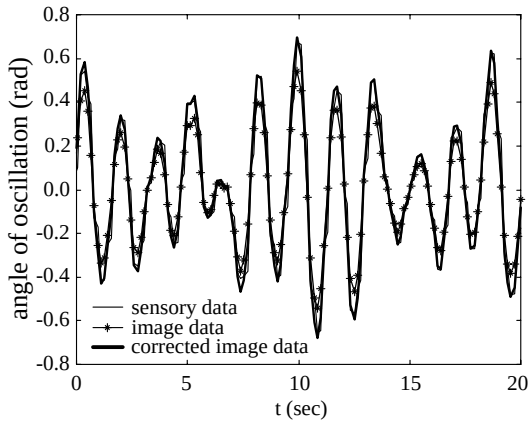

Fig. 8 Plots of image data against sensory data.

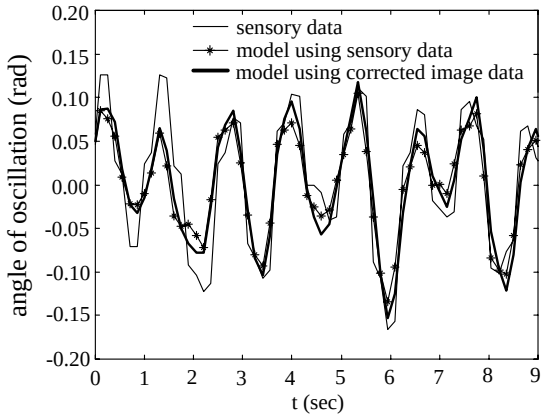

Fig. 9 Plots of linear models of the CPP system.

$$
\begin{aligned}
N(s) &= -0.05101s^{10} - 22.34s^9 + 1452s^8 - 1.515\times10^4 s^7 \\
&\quad - 6.373\times10^4 s^6 - 3.401\times10^7 s^5 + 2.698\times10^8 s^4 \\
&\quad + 1.611\times10^9 s^3 + 7.649\times10^9 s^2 + 7.53\times10^{10} s - 2.975\times10^{10} \\
D(s) &= s^{10} + 216s^9 + 2.182\times10^4 s^8 + 1.322\times10^6 s^7 \\
&\quad + 4.644\times10^7 s^6 + 1.096\times10^9 s^5 + 4.693\times10^9 s^4 \\
&\quad + 4.271\times10^{10} s^3 + 1.167\times10^{11} s^2 + 3.405\times10^{11} s + 6.218\times10^{11}
\end{aligned}
\tag{23}
$$

$$
\begin{aligned}
N(s) &= -0.03771s^{10} + 2.238s^9 - 156.7s^8 + 1412s^7 \\
&\quad - 5.541\times10^4 s^6 + 5.608\times10^5 s^5 - 4.758\times10^6 s^4 \\
&\quad + 1.003\times10^8 s^3 - 1.103\times10^8 s^2 + 2.68\times10^9 s - 8.344\times10^8 \\
D(s) &= s^{10} + 46.35s^9 + 3559s^8 + 7.59\times10^4 s^7 \\
&\quad + 1.331\times10^6 s^6 + 1.969\times10^7 s^5 + 1.327\times10^8 s^4 \\
&\quad + 7.772\times10^8 s^3 + 3.524\times10^9 s^2 + 7.092\times10^9 s + 2.004\times10^{10}
\end{aligned}
\tag{24}
$$

4.1.1 Linear CPP

The CPP system can be assumed linear when the angles of oscillation are small, i.e. within ±0.2 rad. A black-box model of 10th order has been assumed to represent the linear CPP system. The Identification Toolbox of MATLAB™ has been used to accomplish the model identification. Models obtained from sensory data and corrected image data are expressed in (23) and (24) respectively. Figure 9 shows the sensory data plotted against the model

obtained from sensory data and corrected image data. Curves indicate the agreement of the oscillation mode and amplitude.

4.1.2 Nonlinear CPP

The CPP system is considered nonlinear when the angles of oscillation are large. The systems can be described by (11) and (12) in which all the parameters except *M* are known. However, the force that directly applies to the cart is not known. This is because the cart is driven by the belt that swings up-and-down all the time. This belt receives random excitation from the motor. The problem now becomes an identification of the forcing function, *f*. The force, *f*, is assumed the 7th-order polynomial of the motor input, *u*, as expressed in (25). In this case, it is not possible to apply any existing conventional methods of identification. We thus apply the search method namely the adaptive tabu search (ATS) [11] to identify the following parameters: M, a_7, a_6,…, and a_0 of the forcing function, *f*. Readers can find a brief description of the ATS in the Appendix.

The ATS is applied to search for the CPP nonlinear model parameters. The stop criteria are the cost J (sum-squared error, SSE, between the observed data and the models) ≤ 1.32 or the maximum search rounds of 10,000. We conducted 1,000 trials with random initial solutions to obtain average search results. Using the sensory data, the ATS provided the solutions with an average J = 1.31, average search rounds of 693.40, and consumed 76.18 seconds of average search time. Using the corrected image data, the ATS provided the solutions with an average J = 1.31, average search rounds of 726.50, and consumed 78.03 seconds of average search time. Models parameters obtained from the ATS are shown in Table 1. Figure 10 shows the sensory data plotted against the models obtained from the sensory data, and the corrected image data. The curves illustrate satisfactory results, although the amplitude errors are still great. The amplitude errors can be decreased by attempting to model the force, *f*, more accurately. This point is still left open.

$$f = a_7 u^7 + a_6 u^6 \cdots + a_1 u + a_0 \qquad (25)$$

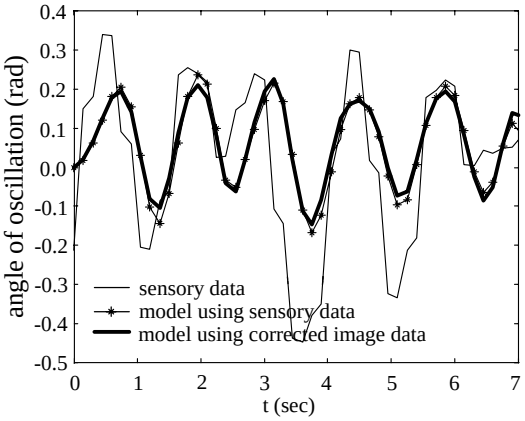

Fig. 10 Plots of nonlinear models of CPP system.

4.2 Identification of the VTS

In this section, the effectiveness of our approach is demonstrated to identify model parameters of the VTS system, on which it is not possible to install traditional sensors, since the tube is small and soft. The VTS has a non-uniform force, *S*, exerted by the motor's shaft. Regarding to Figure 4, the tube has length l = 61 cm, and diameter d = 3.5 mm. The tube is coupled to the motor shaft, and a connector moving freely. The distance between the shaft and the connector is 60 cm.

Figure 11 illustrates the VTS set up. Two VDO cameras are installed in perpendicular to the *x*-*y*, and the *z*-*x* planes, respectively. The first camera is on the *z* axis, and the second one is on the *y* axis. The cameras are Sony Digital Handycam DCR-VX1000E having lens of 5.9-59 mm. Two VDO captures used in our experiments are One Point Cap-IT2000 with 25 frames per second (fps). Two computers to store the recorded images are Pentium II, 400 MHz, 64 Mbyte RAM.

To lessen the image distortion and to acquire the system dynamic synchronously, both cameras require careful calibration, and synchronization. For camera calibration, we use the effective method proposed by Heikkila and Silven [12]. The method utilizes optimization, and the direct linear transform model. For synchronization of the cameras, we use a single toggle switch to start and stop image capture.

Table 1. Model parameters of nonlinear CCP system.

	M (*kg*)	a_7	a_6	a_5	a_4	a_3	a_2	a_1	a_0
Model parameters obtained from sensory data	0.901	4.09	6.99	-1.83	-5.60	-4.99	-2.33	2.49	-0.15
Model parameters obtained from corrected image data	0.905	4.36	6.92	-1.97	-5.29	-4.99	-2.55	2.47	-0.14

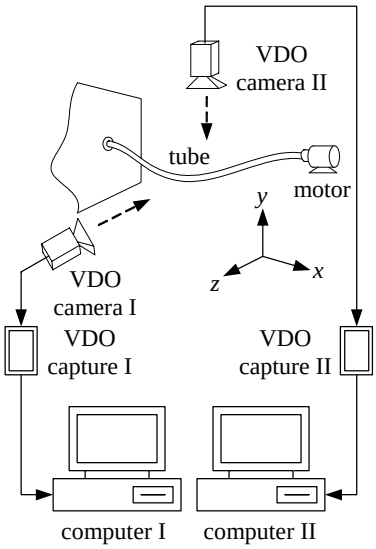

Fig. 11 The VTS set up.

The image files synchronously captured by two cameras are converted to ".avi" files, and then to ".bmp" files. The time interval between two consecutive images is equivalent to a sampling interval of 0.04 sec. The system's sequences of images are captured and processed to extract the most necessary information for the system identification, i.e. tube positions in the corresponding planes. The data representing the tube dynamic in response to the motor's random excitation can be extracted from the recorded images.

In order to locate the tube positions, color segmentation technique is employed. Now, the object of interest is the tube. So, it is assigned a color different from other objects. The color segmentation technique is also applied to segment out the tube from the scene of every single image frame. The image sequences are recorded in RGB format. Ranges of R, G and B values are firstly calculated for each object's color. The color threshold technique is applied to segment each object based on the information of these RGB parameters. Figure 12 shows a result of the color segmentation obtained from the second camera. From the segmented image, the tube positions (in pixel unit) are firstly computed and then converted into VTS parameters (actual tube positions) of the corresponding planes. Figure 13 illustrates some tube positions in the *z*-*x* plane obtained from the second camera before and after calibration. Satisfactory results are obtained from the camera calibration procedure.

The generalized models in (21) and (22) are modified to represent the tube dynamic in the *x*-*y*, and the *z*-*x* planes, respectively. Identification can be conducted for each plane separately. In the *x*-*y* plane, the generalized models can be modified to describe the VTS dynamic as expressed in (26) and (27), where the force, S, is substituted by F, σ is substituted by μ which is the tube mass per unit length in the x axis, g_y is replaced by $g = 9.81$ m/s^2, and $z(x,y,t)$ can be rewritten as $y(x,t)$. We get $\frac{\partial^2 z}{\partial t^2} = \frac{\partial^2 y}{\partial t^2}$, $\frac{\partial^2 z}{\partial x^2} = \frac{\partial^2 y}{\partial x^2}$, and $\frac{\partial^2 z}{\partial y^2} = 0$. The parameters μ, K_M, and K_D, of the VTS need to be identified.

$$\frac{\partial^2 y}{\partial t^2} = \frac{F}{\mu}\left(\frac{\partial^2 y}{\partial x^2}\right) - g \tag{26}$$

$$F = K_D K_M u \tag{27}$$

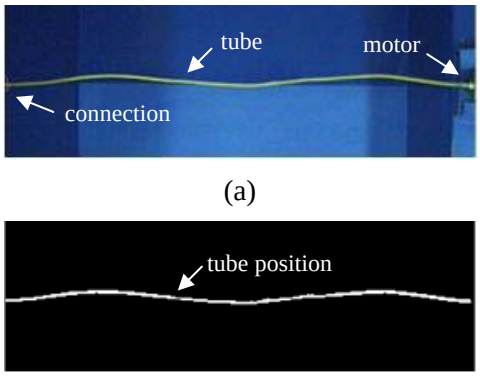

Fig. 12 Color segmentation of the VTS,
(a) recorded-undistorted image
(b) segmented image.

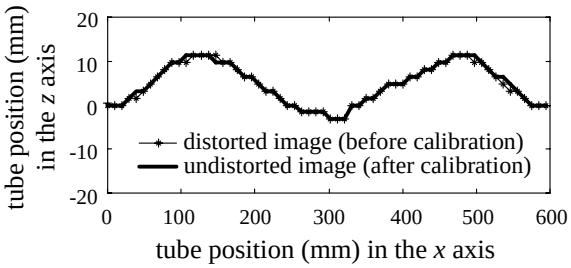

Fig 13. Tube positions in the *z*-*x* plane.

By applying the ATS, the stop criteria are the cost J (mean-squared error, MSE, between the observed positions and the models) ≤ 23.26 or the maximum search rounds of 1,000. We conducted 1,000 trials with random initial solutions to obtain average search results. The ATS provided the solutions with an average J = 23.25, average search rounds of 10.19, and consumed 8.83 seconds of average search time. The following model parameters are obtained: μ = 0.0064 kg/m, K_D =

0.022, and K_M = 0.024. Figure 14 illustrates some of the model plotted against the observed positions in the *x*-*y* plane. The results obtained are highly satisfactory.

In the *z*-*x* plane, the generalized models can be modified to describe the VTS dynamic as expressed in (28) and (29), where the force, *S*, is substituted by *F*, σ is substituted by μ which is the tube mass per unit length in the *x* axis, and $z(x,y,t)$ can be rewritten as $z(x,t)$. We can get $\frac{\partial^2 z}{\partial t^2} = \frac{\partial^2 z}{\partial t^2}$, $\frac{\partial^2 z}{\partial x^2} = \frac{\partial^2 z}{\partial x^2}$, and $\frac{\partial^2 z}{\partial y^2} = 0$. In this case, g_y is replaced by zero because the direction of gravity g_y is in perpendicular to the *z*-*x* plane. Thus, the parameters μ, K_M, and K_D, need to be identified.

$$\frac{\partial^2 z}{\partial t^2} = \frac{F}{\mu}\left(\frac{\partial^2 z}{\partial x^2}\right) \tag{28}$$

$$F = K_D K_M u \tag{29}$$

By applying the ATS to search such the parameters, the stop criteria are the cost *J* (MSE) ≤ 32.38 or the maximum search rounds of 1,000. Again, 1,000 trials with random initial solutions were conducted. The ATS provided the solutions with an average *J* = 32.37, average search rounds of 7.18, and consumed 5.59 seconds of average search time. The following model parameters are obtained: μ = 0.0065 kg/m, K_D = 0.022, and K_M = 0.020. The system parameters obtained by the ATS highly agree with those obtained from the *x*-*y* plane identification. Figure 15 illustrates some of the model plotted against the observed positions in the *z*-*x* plane. The simulation results are satisfactory, although some amplitude errors occur noticeably because the gravity is set as zero. These errors affect the setting of the cost *J* barred by 32 approximately as the readers might observe this. The amplitude errors can be decreased by using an additional camera (or more, if necessary) installed in an oblique plane. The generalized models of the VTS should correspondingly modified. This point is still left open.

5 Conclusion

A new approach to system identification via image processing technique has been described. VDO cameras play a substantial replacement for traditional sensors. Dynamical information of the system can be extracted from the recorded images using simple color segmentation, and color threshold techniques. The paper has demonstrated this new approach to obtain linear and nonlinear model's parameters of the cart-plus-pendulum (CPP) system as well as those of the PDE models of the vibrating tube system (VTS). Based on the image data, conventional regression-identification techniques are applied to identify linear model's parameters of the cart-plus-pendulum system, while the adaptive tabu search (ATS) is applied to identify nonlinear model's parameters of the cart-plus-pendulum system, and PDE model's parameters of the vibrating tube system. The usefulness and practicality of our innovative approach have been confirmed by the experimental results.

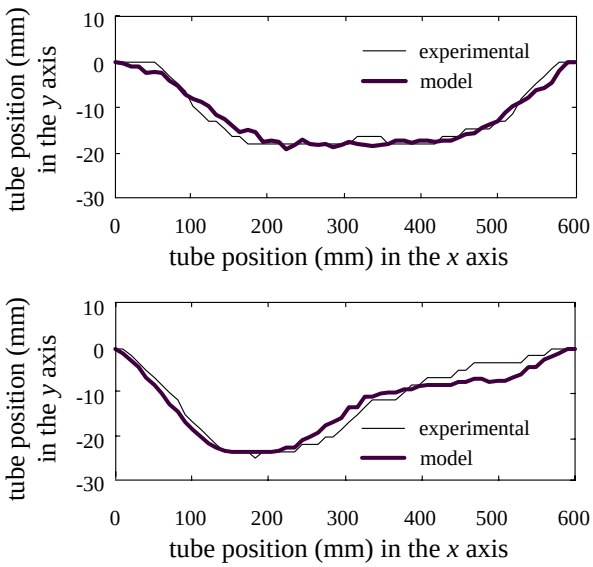

Fig 14. Model plotted against the observed tube positions in the *x*-*y* plane.

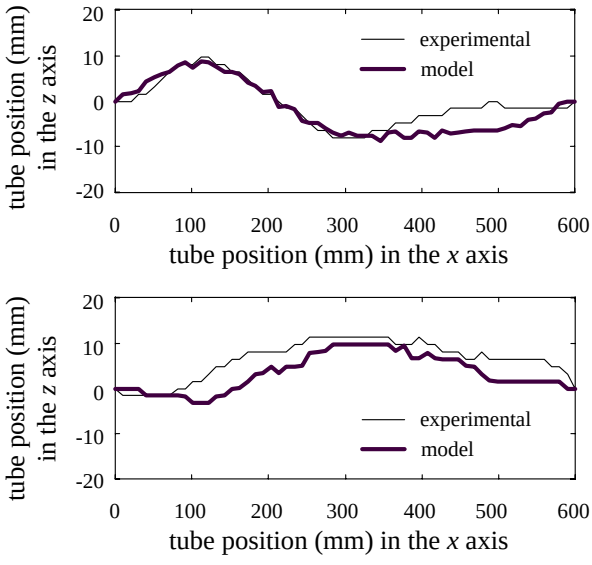

Fig 15. Model plotted against the observed tube positions in the *z*-*x* plane.

6 Appendix: The ATS Method

Based on iterative neighborhood search approach, the ATS method is one of the efficient AI search techniques. With the tabu list (TL), the ATS can record a history of solution movements which may lead to a new direction that could escape a local minimum entrapment. To enhance its convergence, the ATS method has two additional mechanisms, namely back-tracking (BT) and adaptive-radius (AR). The flow diagram in Figure 16 describes the ATS algorithm.

When the number of solution cycling is equal to the maximum solution-cycling allowance, the BT mechanism is active. This mechanism selects one of the solutions stored in the TL as an initial solution for the next search round to enable a new search direction. The AR mechanism is active when a current solution is relatively close to a local minimum. The search radius is decreased in accordance with the best solution found. The less the cost function, the smaller the radius. With these two mechanisms, a solution obtained by the ATS rapidly converges to the global minimum. Readers can find the convergence analysis and performance evaluation of the ATS method in [11].

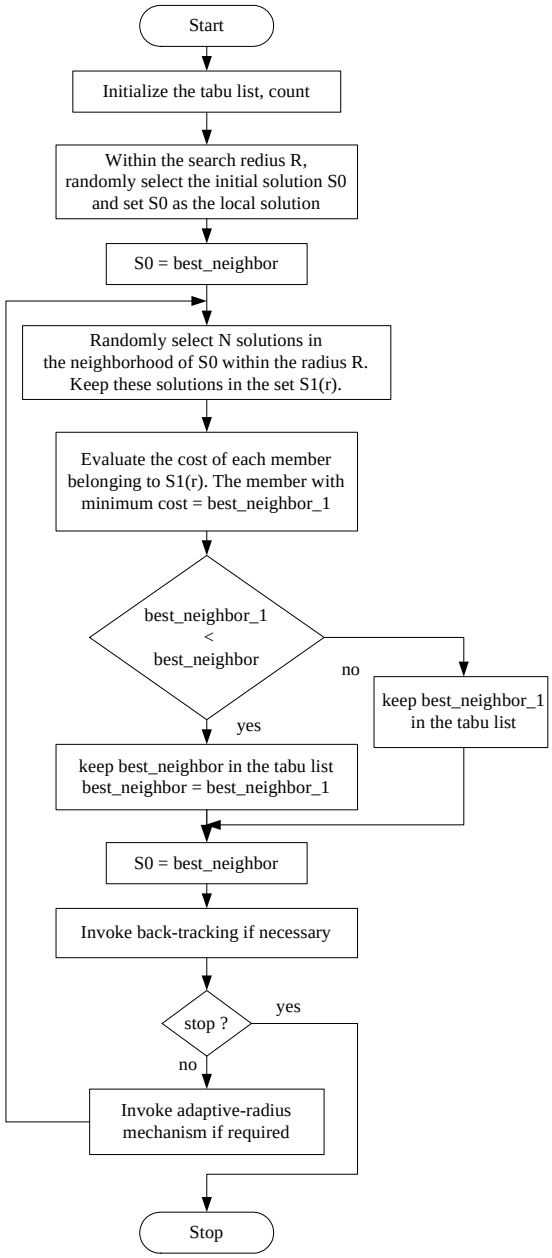

Fig. 16 Algorithm of the ATS method.

References:

[1] J.W. Roach and J.K. Aggarwal, Determining the Movement of Objects from a Sequence of Images, *IEEE Trans. Pattern Analysis and Machine Intelligence*, Vol. PAMI-2, No. 6, 1980, pp. 554-562.

[2] J. Weng, T.S. Huang, and N. Ahuja, 3-D Motion Estimation, Understanding, and Prediction from Noisy Image Sequences, *IEEE Trans. Pattern Analysis and Machine Intelligence*, Vol. PAMI-9, No. 3, 1987, pp. 370-389.

[3] J.K. Aggarwal and N. Nandhakumar, On the Computation of Motion from Sequences of Images-A Reviews, *Proc. IEEE*, No. 76, 1988, pp. 917-935.

[4] R.R. Forstor, K.C. Jezek, and H.G. Sohn, Analysis of Glacier Flow Dynamics from Preliminary RADARSAT InSAR data, *Proc. IEEE Int. Symposium on Geoscience and Remote Sensing*, 1998, pp. 2225-2227, USA, WA: Seattle.

[5] B.K. Ghosh and E.P. Loucks, A Realization Theory for Perspective Systems with Applications to Parameter Estimation Problems in Machine Vision, *IEEE Trans. Automatic Control*, Vol. 41, No. 12, 1996, pp. 1706-1722.

[6] B.K. Ghosh, H. Inaba, and S. Takahashi, Identification of Riccati Dynamic under Perspective and Orthographic Observations, *IEEE Trans. Automatic Control*, Vol. 45, No. 7, 2000, pp. 1267-1278.

[7] S. Sujitjorn, A. Srikaew, D. Puangdownreong, K. Attakitmongcol, and P. Totarong, Model Identification using Image Processing Technique, *Proc. CCCT'03 Int. Conf. on Computer, Communication and Control Technologies*, Vol. 3, 2003, pp. 530-535, USA, Florida.

[8] H.-C. Chung, J. Liang, S. Kushiyama, and M. Shinozuka, Digital Image Processing for Non-Linear System Identification, *Non-Linear Mechanics*, Vol. 39, 2004, pp. 691-707.

[9] A.M. Bloch, N.E. Leonard, and J.E. Marsden, Controlled Lagrangians and the Stabilization of Mechanical System I: the First Matching Theorem. *IEEE Trans. Automatic Control*, Vol. 45, No. 12, 2000, pp. 2253-2270.

[10] A.P. French, *Vibrations and Waves*, M.I.T Introductory Physics Series, Chapman & Hall, 1992.

[11] D. Puangdownreong, T. Kulworawanichpong and S. Sujitjorn, Finite Convergence and Performance Evaluation of Adaptive Tabu Search, *Lecture Notes in Computer Science (online)*, Springer-Verlag, 2004.

[12] J. Heikkila and O. Silven, A Four-Step Camera Calibration Procedure with Implicit Image Correction, *Proc. IEEE Int. Conf. on Computer Vision and Pattern Recognition*, 1997, pp. 1106-1112.